ACS OMEGA

Open Access

http://pubs.acs.org/journal/acsodf

Article

Out-of-Plane Longitudinal Sound Speed Determination in GaS by Broadband Time-Domain Brillouin Scattering

Watheq Al-Basheer,* Christian Viernes, Ruofei Zheng, Sam Netzke, Kostyantyn Pichugin, and German Sciaini*

Cite This: *ACS Omega* 2024, 9, 47475−47479

Read Online

ACCESS | Metrics & More | Article Recommendations

ABSTRACT: Two-dimensional semiconducting gallium sulfide (GaS) has garnered notable interest for its distinct structural and optical properties, which position it as a promising candidate material for various applications ranging from photodetection and photovoltaics to nonlinear frequency conversion. In this work, we determined the out-of-plane longitudinal sound velocity, v_L, via impulsive time-domain femtosecond broadband Brillouin scattering measurements performed on a single flake-like GaS crystal. We obtained a value v_L= (3140 ± 20) m/s, which yields an out-of-plane compressive elastic constant, C_{33}= (38.1 ± 0.5) GPa.

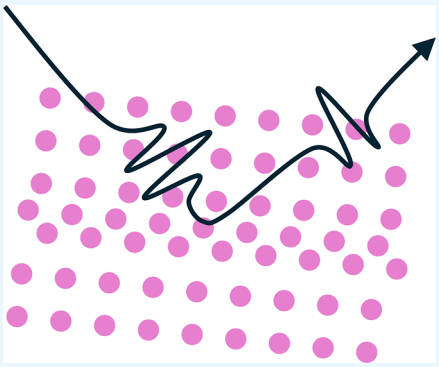

1. INTRODUCTION

The advancements in the field of ultrafast and high-energy laser pulses,[1−5] combined with improvements in pump−probe excitation and detection schemes, have led to the development of multiple experimental approaches for the generation and observation of coherent acoustic phonons in diverse materials.[6−18] The use of ultrashort laser pulses to produce coherent acoustic waves, followed by detection via time-delayed ultrashort probe pulses, originated in the 1980s, establishing picosecond ultrasonics.[6,7] Over time, numerous investigations have explored the propagation of acoustic phonons through both opaque and transparent media using various optical pump−probe configurations.[9−18] As the photoelastic interaction between ultrashort pulses and transparent crystals satisfies Brillouin scattering (BS) criteria, this variant of picosecond ultrasonics has been termed time-domain Brillouin scattering (TDBS).[19]

In TDBS, the rapid thermal expansion resulting from the intense and impulsive laser absorption initiates a coherent acoustic wave.[20−24] This wave propagates from the surface into the bulk, moving at a speed that depends on the material's elastic characteristics. The acoustic pulse serves as a dynamic reflecting interface, causing temporal changes in the local density (i.e., dielectric function), which are tracked using a probe pulse.[21−27] Our TDBS approach utilizes broad-band white-light probe pulses paired with optical heterodyne detection. Figure 1a illustrates the geometrical arrangement in which the refracted and reflected portion of the probe pulse (ray 2), which interacts with moving acoustic wave, interferes

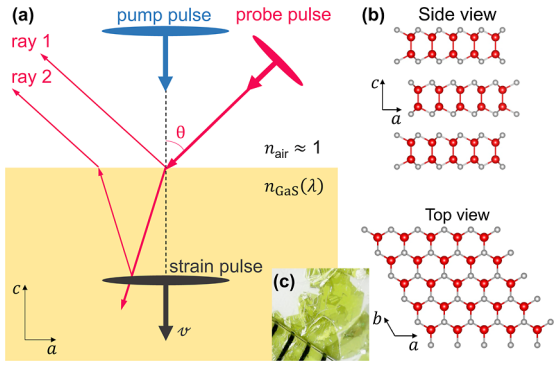

Figure 1. (a) Schematic of the ray propagation geometry in the experimental setup, with the pump beam impinging perpendicularly on the crystal's surface, while the probe beam is angled at approximately $\theta \approx 10°$. Also depicted is the moving acoustic pulse, which acts as a reflective boundary. (b) Side and top views of the GaS crystalline structure. (c) Photograph of GaS sample; distance between ruler divisions = 1 mm.

Received: June 21, 2024
Revised: November 7, 2024
Accepted: November 15, 2024
Published: November 21, 2024

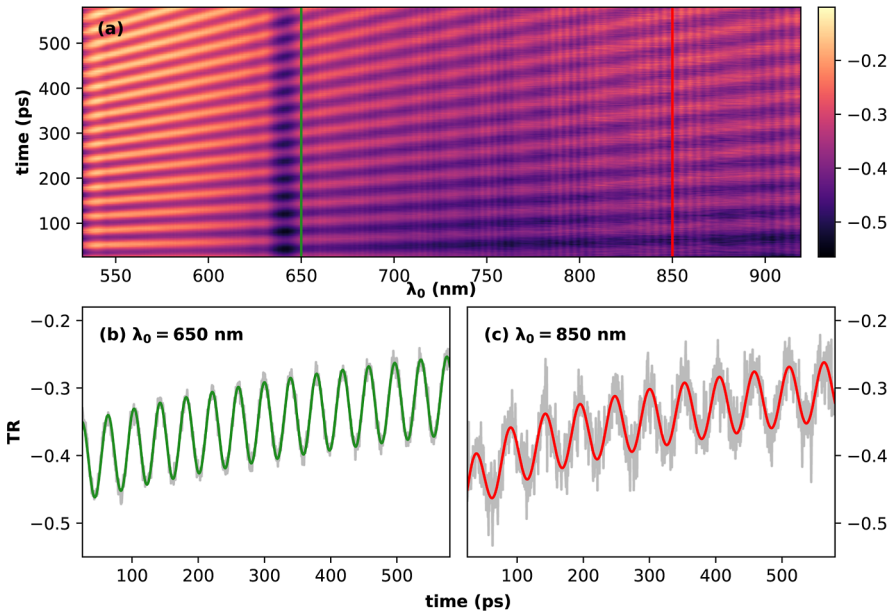

Figure 2. (a) Broadband, time-resolved transient reflectivity spectrum attained at room temperature with a time step of 500 fs. Panels (b,c) display two temporal signals obtained at probe wavelengths of 650 and 850 nm, respectively; the wavelengths are also indicated as vertical lines in (a). The experimental data are depicted as gray, while fittings using eq 2 are shown in panels (b,c) as green and red traces, respectively. Incident excitation fluence = 1.5 mJ cm^{-2}.

with the fraction reflected at the air-material interface (ray 1). Moreover, broadband detection allows precise determination of the out-of-plane longitudinal sound speed, achieved through linear regression across a wide wavelength range.

This work focused on the acoustic study of a high-quality single flake-like two-dimensional (2D) GaS crystal to determine the out-of-plane longitudinal sound speed via TDBS. The latter represents the compressive wave's velocity perpendicular to the plane of the crystal's 2D layers. GaS, a group-III monochalcogenide, has garnered attention due to its remarkable semiconducting properties.[28] Additionally, its strong UV absorption and effective carrier mobility make it well-suited for photonic and optoelectronic applications like fast UV photodetectors,[29−33] hydrogen evolution catalysis,[34] field-effect transistors,[35] energy storage,[36,37] gas sensing,[38,39] and nonlinear optics.[40,41] Previous studies have investigated GaS's structure and optical properties,[42−46] while BS has been employed to ascertain its elastic properties under varying chemical compositions and pressures.[47−52] Extending BS to the time domain in this work offers a direct measure of the out-of-plane longitudinal sound speed, showcasing the combined benefits of frequency- and time-domain BS methods.

2. EXPERIMENTAL SECTION

The GaS sample studied was a high-quality, flake-like β-phase single crystal measuring roughly 6 mm laterally and less than 0.5 mm thick, with purity exceeding 99.995%, sourced from HQ Graphene. Prior to mounting, the crystal underwent gentle mechanical exfoliation to clean its surface. As a stable 2D layered diamagnetic semiconductor, β-GaS exhibits an indirect bandgap of 2.53 eV at room temperature[42] and a hexagonal unit cell[53] with parameters of $a = b = 0.359$ nm, $c = 1.549$ nm, and $\alpha = \beta = 90°$, $\gamma = 120°$. Figure 1b shows the crystal's structure from both side and top perspectives, illustrating GaS layers containing two covalently bonded Ga atoms between two layers of S atoms with a distinct stacking sequence of S−Ga−Ga−S along the c-axis.[54] The layers are held together by weak van der Waals forces, contributing to the thermal and mechanical stability of the beta phase compared to other GaS phases.[54]

Our experimental pump−probe setup employs a Pharos-SP femtosecond laser from light conversion, delivering 170 fs pulses at a 6 kHz repetition rate with a central wavelength of 1030 nm. To generate pump laser pulses at λ_{pump} = 320 nm (3.87 eV), we utilized optical parametric amplification, followed by second harmonic frequency conversion. For differential transient reflectivity measurements, the pump beam was modulated using a mechanical chopper operating at half of the acquisition rate. The setup ensured stable signal detection by creating a pump beam spot size of about 300 μm at full-width half-maximum (fwhm) at the crystal's surface using a long focal length lens. Ultraviolet excitation well above the β-GaS bandgap effectively eliminated the need for a thin transducing metallic layer.[55] Broadband probe pulses were generated by directing a small portion of the initial laser output through a 3 mm thick yttrium aluminum garnet crystal, filtering out the remaining 1030 nm component with a bandpass filter. This process produced a white light supercontinuum covering λ_{probe} = 500−950 nm, which was used to capture transient reflectivity variations. A short focal length lens focused the probe beam to approximately 50 μm at the fwhm on the sample surface.

Figure 1a depicts the arrangement of pump and probe beams relative to the 2D crystal layers. The pump beam strikes the surface perpendicularly, while the probe beam is angled at approximately $\theta \approx 10°$. The reflected and refracted probe beams, labeled as ray 1 and ray 2, respectively, interact in distinct ways: ray 2 reflects from the acoustic pulse moving within the material and then interferes with ray 1 at the detector. Given the much higher speed of light compared to that within the medium, the detection method operates in a stroboscopic fashion, capturing dynamic changes as they occur. An optical delay stage positioned along the probe beam path

https://doi.org/10.1021/acsomega.4c05738
ACS Omega 2024, 9, 47475−47479

was used to control the optical path difference between the pump and probe pulses. The transient reflectivity signals were recorded with a frame transfer rate of 1 kHz using a dispersive spectrometer.

3. RESULTS AND DISCUSSION

The Brillouin frequency, denoted as ν_B, results from alternating constructive and destructive interference effects between ray 1 and ray 2 and can be expressed as[18,56,57]

$$\nu_B = 2\nu_L \frac{\sqrt{n^2 - \sin^2\theta}}{\lambda_0} \quad (1)$$

where λ_0 is the probe pulse wavelength in air, ν_L is the out-of-plane longitudinal sound speed, and n is the real part of the GaS crystal's refractive index. The detailed derivation of this equation via ray tracing is provided in ref 18. Equation 1 facilitates direct extraction of ν_B from the transient reflectivity profiles measured over a broad wavelength range, offering valuable insights into the material's elastic properties.

Figure 2a shows a broadband, time-resolved transient reflectivity spectrum obtained at room temperature. The dominant feature in the TDBS signal is a long-lived oscillation, which overlaps with a slowly changing background caused by the dynamics of the photoexcited carriers within GaS.

Figure 2b,c display specific time slices of the broadband transient reflectivity spectrum at probe wavelengths λ_0 = 650 and 850 nm, respectively. In these graphs, the oscillatory gray traces represent the raw experimental data, while the green and red solid lines correspond to fitted models. These fits are based on the phenomenological model described in eq 2

$$S(t) = A_1(1 - e^{-(t-t_1)/\tau_1}) + A_2 e^{-(t-t_2)/\tau_2} + A_3 e^{-(t-t_3)/\tau_3}\sin(2\pi\nu_B t + \varphi) + C \quad (2)$$

Equation 2 shows the determination of ν_B for each probed wavelength, λ_0, through a set of adjustable parameters: time constants $\tau_{i=1,2,3}$, amplitudes $A_{i=1,2,3}$, initial time offsets $t_{i=1,2,3}$, phase φ (relative to time zero), and an offset C, which represents the long-term signal asymptote. The first two terms describe the background signal caused by carrier dynamics over time, while the third term, a damped sinusoidal function, is key for identifying ν_B. The damping component accounts for effects like decoherence and absorption that primarily affect ray 2, especially as probe photon energies approach GaS's bandgap.

A linear correlation emerges from eq 1 when the measured BS frequencies, ν_B, are plotted as a function of $\frac{n^*}{\lambda_0} = \frac{\sqrt{n^2 - \sin^2\theta}}{\lambda_0}$. Refractive indexes from the literature,[58] spanning the range of probe wavelengths used, were modeled using Cauchy's equation, $n(\lambda_0) = A + B/\lambda_0^2 + C/\lambda_0^4$. Given that GaS exhibits uniaxial birefringence, the ordinary refractive index component is relevant in this optical setup. This configuration facilitates a straightforward extraction of the out-of-plane longitudinal sound speed from the slope of the linear fit, which equals $2\nu_L$.

Figure 3 illustrates the linear relationship between ν_B and $\frac{n^*}{\lambda_0}$, derived from eq 1 and based on the standard beam propagation model, which assumes negligible absorption effects on ray 2. According to Chang et al.,[59] this assumption holds when the ratio of the imaginary to real components of the refractive index (k/n) is less than 0.07. As reported by

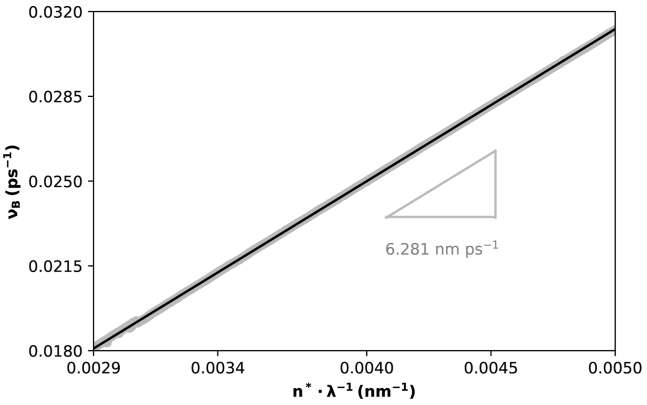

Figure 3. Linear correlation between Brillouin frequency, ν_B, and the ratio $n^*(\lambda_0)/\lambda_0$ from λ_0 = 500 to 700 nm. The gray trace represents experimental data; the black line is the linear fit with a slope of $2\nu_L$ = 6.281 nm/ps and a standard deviation of 0.001 nm/ps.

McMath et al.,[58] the maximum value of k/n across the wavelength range used in this study is approximately 0.01, which supports the validity of the propagation model and eq 1.

The slope of the linear fit in Figure 3 was determined to be $2\nu_L = 6.281 \pm 0.001$ nm ps^{-1}, corresponding to an out-of-plane longitudinal sound speed of $\nu_L = 3140 \pm 20$ m/s in GaS. The primary source of error in the evaluation of the sound speed stems from uncertainties related to the incident angle of the probe beam.

Furthermore, when the material's response is perfectly elastic or linear according to Hooke's law, the determined out-of-plane longitudinal speed of sound is related to the compressive elastic constant $C_{33} = \rho\nu_L^2$, where ρ = 3.86 g/cm^3 is the mass density of GaS.[60] By substitution of these values, the elastic constant C_{33} was calculated to be (38.1 ± 0.5) GPa. This value is consistent with those reported earlier using frequency-domain BS by Polian et al.[47,48] (37.7 GPa), Honma et al.[49] (37.9 GPa), and Fischer et al.[50] (38.5 GPa). Additionally, it closely matches the 38.5 GPa reported value by Gatulle et al.,[51,52] using ultrasonic waves on large, several-millimeter crystals, and the 36.4 GPa by Powell et al.[61] using neutron scattering.

4. CONCLUSIONS

The excellent agreement between the values of C_{33} reported from BS experiments in the frequency domain[47−50] and our result, obtained from $C_{33} = \rho\nu_L^2$, confirms that GaS's response to intense impulsive fs photoexcitation remains within the linear elastic regime, where stress is proportional to strain. This finding supports the use of this nondestructive, all-optical technique for determining the elastic constants of more valuable and smaller 2D layered materials, which are unsuitable for conventional mechanical testing or acoustic methods that require much larger specimens.[51,52]

AUTHOR INFORMATION

Corresponding Authors

Watheq Al-Basheer − *Department of Physics, King Fahd University of Petroleum & Minerals, Dhahran 31261, Saudi Arabia; Interdisciplinary Research Center of Membranes and Water Security, King Fahd University of Petroleum & Minerals, Dhahran 31261, Saudi Arabia;* orcid.org/0000-0002-2100-9333; Email: watheq@kfupm.edu.sa

https://doi.org/10.1021/acsomega.4c05738
ACS Omega 2024, 9, 47475−47479

German Sciaini − *The Ultrafast Electron Imaging Lab, Department of Chemistry, and Waterloo Institute for Nanotechnology, University of Waterloo, Waterloo N2L 3G1, Canada;* orcid.org/0000-0002-2120-3996; Email: gsciaini@uwaterloo.ca

Authors

Christian Viernes − *The Ultrafast Electron Imaging Lab, Department of Chemistry, and Waterloo Institute for Nanotechnology, University of Waterloo, Waterloo N2L 3G1, Canada*

Ruofei Zheng − *The Ultrafast Electron Imaging Lab, Department of Chemistry, and Waterloo Institute for Nanotechnology, University of Waterloo, Waterloo N2L 3G1, Canada*

Sam Netzke − *The Ultrafast Electron Imaging Lab, Department of Chemistry, and Waterloo Institute for Nanotechnology, University of Waterloo, Waterloo N2L 3G1, Canada*

Kostyantyn Pichugin − *The Ultrafast Electron Imaging Lab, Department of Chemistry, and Waterloo Institute for Nanotechnology, University of Waterloo, Waterloo N2L 3G1, Canada*

Complete contact information is available at: https://pubs.acs.org/10.1021/acsomega.4c05738

Notes

The authors declare no competing financial interest.

■ ACKNOWLEDGMENTS

G.S. acknowledges the support of the National Science and Engineering Research Council of Canada, the Canada Foundation for Innovation, and the Ontario Research Foundation. W. Al-Basheer is grateful to King Fahd University of Petroleum and Minerals for funding under Research Grant (#ISP231-PHYS-795).

■ REFERENCES

(1) Knox, W. H.; Downer, M. C.; Fork, R. L.; Shank, C. V. Amplified femtosecond optical pulses and continuum generation at 5-kHz repetition rate. *Opt. Lett.* **1984**, *9* (12), 552−554.

(2) Strickland, D.; Mourou, G. Compression of Amplified Chirped Optical Pulses. *Opt. Commun.* **1985**, *56*, 219−221.

(3) Nuss, M. C.; Leonhardt, R.; Zinth, W. Stable operation of a synchronously pumped colliding-pulse mode-locked ring dye laser. *Opt. Lett.* **1985**, *10* (1), 16−18.

(4) French, P. M. W.; Williams, J. A. R.; Taylor, J. R. Femtosecond pulse generation from a titanium-doped sapphire laser using nonlinear external cavity feedback. *Opt. Lett.* **1989**, *14* (13), 686−688.

(5) Nickel, D.; Kühlke, D.; von der Linde, D. Multipass dye-cell amplifier for high-repetition-rate femtosecond optical pulses. *Opt. Lett.* **1989**, *14* (1), 36−38.

(6) Nelson, K. A. Stimulated Brillouin scattering and optical excitation of coherent shear waves. *J. Appl. Phys.* **1982**, *53*, 6060−6063.

(7) Thomsen, C.; Strait, J.; Vardeny, Z.; Maris, H. J.; Tauc, J.; Hauser, J. J. Coherent phonon generation and detection by picosecond light pulses. *Phys. Rev. Lett.* **1984**, *53*, 989−992.

(8) Devos, A.; Côte, R. Strong oscillations detected by picosecond ultrasonics in silicon: Evidence for an electronic-structure effect. *Phys. Rev. B* **2004**, *70*, 125208.

(9) Makarona, E.; Daly, B.; Im, J.-S.; Maris, H.; Nurmikko, A.; Han, J. Coherent generation of 100 GHz acoustic phonons by dynamic screening of piezoelectric fields in AlGaN/GaN multilayers. *Appl. Phys. Lett.* **2002**, *81*, 2791−2793.

(10) Matsuda, O.; Wright, O. B.; Hurley, D. H.; Gusev, V.; Shimizu, K. Coherent shear phonon generation and detection with picosecond laser acoustics. *Phys. Rev. B* **2008**, *77*, 224110.

(11) Harb, M.; Peng, W.; Sciaini, G.; Hebeisen, C. T.; Ernstorfer, R.; Eriksson, M. A.; Lagally, M. G.; Kruglik, S. G.; Miller, R. J. D. Excitation of longitudinal and transverse coherent acoustic phonons in nanometer free-standing films of (001) Si. *Phys. Rev. B* **2009**, *79*, 094301.

(12) Zhang, S.; Péronne, E.; Belliard, L.; Vincent, S.; Perrin, B. Three-dimensional acoustic wavefront imaging in anisotropic systems by picosecond acoustics. *J. Appl. Phys.* **2011**, *109*, 033507.

(13) Pontecorvo, E.; Ortolani, M.; Polli, D.; Ferretti, M.; Ruocco, G.; Cerullo, G.; Scopigno, T. Visualizing coherent phonon propagation in the 100 GHz range: A broadband picosecond acoustics approach. *Appl. Phys. Lett.* **2011**, *98*, 011901.

(14) Brivio, S.; Polli, D.; Crespi, A.; Osellame, R.; Cerullo, G.; Bertacco, R. Observation of anomalous acoustic phonon dispersion in $SrTiO_3$ by broadband stimulated Brillouin scattering. *Appl. Phys. Lett.* **2011**, *98*, 211907.

(15) Klieber, C.; Pezeril, T.; Andrieu, S.; Nelson, K. A. Optical generation and detection of gigahertz-frequency longitudinal and shear acoustic waves in liquids: Theory and experiment. *J. Appl. Phys.* **2012**, *112*, 013502.

(16) Pezeril, T. [INVITED] Laser generation and detection of ultrafast shear acoustic waves in solids and liquids. *Opt. Laser Technol.* **2016**, *83*, 177−188.

(17) Rivas, N.; Zhong, S.; Dekker, T.; Cheng, M.; Gicala, P.; Chen, F.; Luo, X.; Sun, Y.; Petruk, A. A.; Pichugin, K.; Tsen, A. W.; Sciaini, G. Generation and detection of coherent longitudinal acoustic waves in ultrathin 1T'-$MoTe_2$. *Appl. Phys. Lett.* **2019**, *115*, 223103.

(18) Gicala, P.; Cheng, M.; Lott, T. S.; Du, K.; Cheong, S.-W.; Petruk, A. A.; Pichugin, K.; Sciaini, G. Time-resolved broadband impulsive stimulated Brillouin scattering in single crystal hematite. *Appl. Phys. Lett.* **2021**, *118*, 264101.

(19) Chiao, R. Y.; Townes, C. H.; Stoicheff, B. P. Stimulated Brillouin Scattering and Coherent Generation of Intense Hypersonic Waves. *Phys. Rev. Lett.* **1964**, *12* (21), 592−595.

(20) Lin, H.-N.; Stoner, R. J.; Maris, H. J.; Tauc, J. Phonon attenuation and velocity measurements in transparent materials by picosecond acoustic interferometry. *J. Appl. Phys.* **1991**, *69*, 3816−3822.

(21) Ballmann, C. W.; Meng, Z.; Traverso, A. J.; Scully, M. O.; Yakovlev, V. V. Impulsive Brillouin microscopy. *Optica* **2017**, *4*, 124−128.

(22) Krug, B.; Koukourakis, N.; Czarske, J. W. Impulsive stimulated Brillouin microscopy for non-contact, fast mechanical investigations of hydrogels. *Opt. Express* **2019**, *27*, 26910−26923.

(23) Krug, B.; Koukourakis, N.; Guck, J.; Czarske, J. W. Nonlinear microscopy using impulsive stimulated Brillouin scattering for high-speed elastography. *Opt. Express* **2022**, *30*, 4748−4758.

(24) O'Connor, S. P.; Doktor, D. A.; Scully, M. O.; Yakovlev, V. V. Spectral resolution enhancement for impulsive stimulated Brillouin spectroscopy by expanding pump beam geometry. *Opt. Express* **2023**, *31*, 14604−14616.

(25) Zhang, X.; Song, H.-Y.; Nie, X. C.; Liu, S.-B.; Wang, Y.; Jiang, C.-Y.; Zhao, S.-Z.; Chen, G.; Meng, J.-Q.; Duan, Y.-X.; Liu, H. Y. Ultrafast hot carrier dynamics of $ZrTe_5$ from time-resolved optical reflectivity. *Phys. Rev. B* **2019**, *99*, 125141.

(26) Wang, Y.; Hurley, D. H.; Hua, Z.; Pezeril, T.; Raetz, S.; Gusev, V. E.; Tournat, V.; Khafizov, M. Imaging grain microstructure in a model ceramic energy material with optically generated coherent acoustic phonons. *Nat. Commun.* **2020**, *11*, 1597.

(27) Gusev, V. E. Contra-intuitive features of time-domain Brillouin scattering in collinear paraxial sound and light beams. *Photoacoustics* **2020**, *20*, 100205.

(28) Gutiérrez, Y.; Dicorato, S.; Dilonardo, E.; Palumbo, F.; Giangregorio, M. M.; Losurdo, M. Stability of Nanometer-Thick Layered Gallium Chalcogenides and Improvements via Hydrogen Passivation. *ACS Appl. Nano Mater.* **2023**, *6*, 20161−20172.

(29) Hu, P. A.; Wang, L. F.; Yoon, M.; Zhang, J.; Feng, W.; Wang, X. N.; Wen, Z. Z.; Idrobo, J. C.; Miyamoto, Y.; Geohegan, D. B.; Xiao, K. Highly Responsive Ultrathin GaS Nanosheet Photodetectors on Rigid and Flexible Substrates. *Nano Lett.* **2013**, *13* (4), 1649−1654.
(30) Yang, S.; Li, Y.; Wang, X.; Huo, N.; Xia, J.-B.; Li, S.-S.; Li, J. High performance few-layer GaS photodetector and its unique photo-response in different gas environments. *Nanoscale* **2014**, *6*, 2582−2587.
(31) Chen, T.; Lu, Y.; Sheng, Y.; Shu, Y.; Li, X.; Chang, R.-J.; Bhaskaran, H.; Warner, J. H. Ultrathin all-2D lateral graphene: GaS: graphene UV photodetectors by direct CVD growth. *ACS Appl. Mater. Interfaces* **2019**, *11*, 48172−48178.
(32) Lu, Y.; Chen, J.; Chen, T.; Shu, Y.; Chang, R.; Sheng, Y.; Shautsova, V.; Mkhize, N.; Holdway, P.; Bhaskaran, H.; Warner, J. H. Controlling defects in continuous 2D GaS films for high-performance wavelength-tunable UV-discriminating photodetectors. *Adv. Mater.* **2020**, *32* (7), 1906958.
(33) Dicorato, S.; Gutiérrez, Y.; Giangregorio, M. M.; Palumbo, F.; Bianco, G. V.; Losurdo, M. Interplay between thickness, defects, optical properties, and photoconductivity at the centimeter scale in layered GaS. *Nanomaterials* **2022**, *12* (3), 465.
(34) Harvey, A.; Backes, C.; Gholamvand, Z.; Hanlon, D.; McAteer, D.; Nerl, H. C.; McGuire, E.; Seral-Ascaso, A.; Ramasse, Q. M.; McEvoy, N.; Winters, S.; Berner, N. C.; McCloskey, D.; Donegan, J. F.; Duesberg, G. S.; Nicolosi, V.; Coleman, J. N. Preparation of gallium sulfide nanosheets by liquid exfoliation and their application as hydrogen evolution catalysts. *Chem. Mater.* **2015**, *27* (9), 3483−3493.
(35) Late, D. J.; Liu, B.; Luo, J. J.; Yan, A. M.; Matte, H. S. S. R.; Grayson, M.; Rao, C. N. R.; Dravid, V. P. GaS and GaSe ultrathin layer transistors. *Adv. Mater.* **2012**, *24*, 3549−3554.
(36) Meng, X.; He, K.; Su, D.; Zhang, X.; Sun, C.; Ren, Y.; Wang, H.-H.; Weng, W.; Trahey, L.; Canlas, C. P.; Elam, J. W. Gallium sulfide-single-walled carbon nanotube composites: High-performance anodes for lithium-ion batteries. *Adv. Funct. Mater.* **2014**, *24*, 5435−5442.
(37) Mishra, P.; Singh, D.; Sonvane, Y.; Ahuja, R. Enhancement of hydrogen storage capacity on co-functionalized GaS monolayer under external electric field. *Int. J. Hydrogen Energy* **2020**, *45* (22), 12384−12393.
(38) Opoku, F.; Akoto, O.; Asare-Donkor, N. K.; Adimado, A. A. Defect-engineered two-dimensional layered gallium sulphide molecular gas sensors with ultrahigh selectivity and sensitivity. *Appl. Surf. Sci.* **2021**, *562*, 150188.
(39) Marvan, P.; Mazánek, V.; Sofer, Z. Shear-force exfoliation of indium and gallium chalcogenides for selective gas sensing applications. *Nanoscale* **2019**, *11*, 4310−4317.
(40) Allakhverdiev, K.; Ismailov, F.; Kador, L.; Braun, M. Second-harmonic generation in GaS crystals. *Solid State Commun.* **1997**, *104* (1), 1−3.
(41) Kato, K.; Umemura, N. Sellmeier equations for GaS and GaSe and their applications to the nonlinear optics in GaSxSe1−x. *Opt. Lett.* **2011**, *36* (5), 746−747.
(42) Ho, C. H.; Lin, S. L. Optical properties of the interband transitions of layered gallium sulfide. *J. Appl. Phys.* **2006**, *100* (8), 083508.
(43) Cai, H.; Gu, Y.; Lin, Y.-C.; Yu, Y.; Geohegan, D. B.; Xiao, K. Synthesis and emerging properties of 2D layered III−VI metal chalcogenides. *Appl. Phys. Rev.* **2019**, *6*, 041312.
(44) Jastrzebski, C.; Olkowska, K.; Jastrzebski, D. J.; Wierzbicki, M.; Gebicki, W.; Podsiadlo, S. Raman scattering studies on very thin layers of gallium sulfide (GaS) as a function of sample thickness and temperature. *J. Phys.: Condens. Matter* **2019**, *31*, 075303.
(45) Lu, H.; Chen, Y.; Yang, K.; Kuang, Y.; Li, Z.; Liu, Y. Ultrafast Nonlinear Optical Response and Carrier Dynamics in Layered Gallium Sulfide (GaS) Single-Crystalline Thin Films. *Front. Mater.* **2021**, *8*, 775048.
(46) Zappia, M. I.; Bianca, G.; Bellani, S.; Curreli, N.; Sofer, Z.; Serri, M.; Najafi, L.; Piccinni, M.; Oropesa-Nuñez, R.; Marvan, P.; Pellegrini, V.; Kriegel, I.; Prato, M.; Cupolillo, A.; Bonaccorso, F. Two-Dimensional Gallium Sulfide Nanoflakes for UV-Selective Photoelectrochemical-Type Photodetectors. *J. Phys. Chem. C* **2021**, *125* (22), 11857−11866.
(47) Polian, A.; Besson, J. M.; Grimsditch, M.; Vogt, H. Brillouin scattering from GaS under hydrostatic pressure up to 17.5 GPa. *Appl. Phys. Lett.* **1981**, *38* (5), 334−336.
(48) Polian, A.; Besson, J. M.; Grimsditch, M.; Vogt, H. Elastic properties of GaS under high pressure by Brillouin scattering. *Phys. Rev. B* **1982**, *25*, 2767−2775.
(49) Honma, Y.; Yamada, M.; Yamamoto, K.; Abe, K. Elastic Constants of GaS and GaSe Layered Crystals Determined by Brillouin Scattering. *J. Phys. Soc. Jpn.* **1983**, *52*, 2777−2783.
(50) Fischer, M.; Polian, A.; Chevy, A.; Chervin, J. C. Pressure dependence of the acoustic shear mode in GaS by Brillouin scattering. *Solid State Commun.* **1985**, *56*, 311−313.
(51) Gatulle, M.; Fischer, M.; Chevy, A. Elastic constants of the layered compounds Gas, GaSe, InSe, and their pressure dependence I. Experimental part. *Phys. Status Solidi B* **1983**, *119*, 327−336.
(52) Gatulle, M.; Fischer, M. Elastic Constants of the Layered Compounds GaS, GaSe, InSe, and Their Pressure Dependence. II. Theoretical Part. *Phys. Status Solidi B* **1984**, *121*, 59−71.
(53) Gutiérrez, Y.; Giangregorio, M. M.; Dicorato, S.; Palumbo, F.; Losurdo, M. Exploring the thickness-dependence of the properties of layered gallium sulfide. *Front. Chem.* **2021**, *9*, 781467.
(54) Mosaferi, M.; Abdolhosseini Sarsari, I.; Alaei, M. Band structure engineering in gallium sulfide nanostructures. *Appl. Phys. A: Mater. Sci. Process.* **2021**, *127*, 123.
(55) Bartels, A.; Cerna, R.; Kistner, C.; Thoma, A.; Hudert, F.; Janke, C.; Dekorsy, T. Ultrafast time-domain spectroscopy based on high-speed asynchronous optical sampling. *Rev. Sci. Instrum.* **2007**, *78* (3), 035107.
(56) Ruello, P.; Pezeril, T.; Avanesyan, S.; Vaudel, G.; Gusev, V.; Infante, I. C.; Dkhil, B. Photoexcitation of gigahertz longitudinal and shear acoustic waves in $BiFeO_3$ multiferroic single crystal. *Appl. Phys. Lett.* **2012**, *100*, 212906.
(57) Lejman, M.; Vaudel, G.; Infante, I. C.; Gemeiner, P.; Gusev, V. E.; Dkhil, B.; Ruello, P. Giant ultrafast photo-induced shear strain in ferroelectric $BiFeO_3$. *Nat. Commun.* **2014**, *5*, 4301.
(58) McMath, T. A.; Irwin, J. C. Indices of refraction of GaS and GaSe. *Phys. Status Solidi A* **1976**, *38*, 731−738.
(59) Chang, P. C. Y.; Walker, J. G.; Hopcraft, K. I. Ray tracing in absorbing media. *J. Quant. Spectrosc. Radiat. Transfer* **2005**, *96*, 327−341.
(60) Balkanski, M.; Wallis, R. F. *Semiconductor Physics and Applications*; Oxford University Press: New York, 2000; pp 1−22.
(61) Powell, B. M.; Jandl, S.; Brebner, J. L.; Levy, F. Anisotropic phonon dispersion in GaS. *J. Phys. C: Solid State Phys.* **1977**, *10*, 3039−3049.

https://doi.org/10.1021/acsomega.4c05738
ACS Omega 2024, 9, 47475−47479